Inorg. Chem. **2009**, *48*, 838−845

Comparison of the Reactivity of Bis(μ-oxo)$Cu^{II}Cu^{III}$ and $Cu^{III}Cu^{III}$ Species to Methane

Yoshihito Shiota and Kazunari Yoshizawa*

Institute for Materials Chemistry and Engineering, Kyushu University, Fukuoka 819-0395, Japan

Received February 29, 2008

Methane hydroxylation at the dinuclear copper site of particulate methane monooxygenase (pMMO) is studied by using density functional theory (DFT) calculations. The electronic and structural properties of the dinuclear copper species of bis(μ-oxo)$Cu^{II}Cu^{III}$ and $Cu^{III}Cu^{III}$ are discussed with respect to the C−H bond activation of methane. The bis(μ-oxo)$Cu^{II}Cu^{III}$ species is highly reactive and considered to be an active species for the conversion of methane to methanol by pMMO, whereas the bis(μ-oxo)$Cu^{III}Cu^{III}$ species is unable to react with methane as it is. If a Cu−O bond of the bis(μ-oxo)$Cu^{III}Cu^{III}$ species is cleaved, the resultant $Cu^{III}Cu^{III}$ species, in which only one oxo ligand bridges the two copper ions, can activate methane. However, its energetics for methane hydroxylation is less favorable than that by the bis(μ-oxo)$Cu^{II}Cu^{III}$ species. The DFT calculations show that the bis(μ-oxo)$Cu^{II}Cu^{III}$ species is more effective for the activation of methane than the bis(μ-oxo)$Cu^{III}Cu^{III}$ species. The reactive bis(μ-oxo)$Cu^{II}Cu^{III}$ species can be created either from the electron injection to the bis(μ-oxo)$Cu^{III}Cu^{III}$ species or from the O−O bond cleavage in the μ-η^1:η^2-peroxo$Cu^{I}Cu^{II}$ species.

Introduction

The biological hydroxylation of methane by methane monooxygenase (MMO) is a very interesting and important enzymatic function[1,2] because the direct conversion of methane to methanol is of current interest in applied chemistry. There are two different forms of MMO. One is a cytoplasmic form called soluble methane monooxygenase (sMMO) that has a diiron active site for methane hydroxylation,[3] and the other is an integral membrane form called particulate methane monooxygenase (pMMO) that involves copper active sites.[4,5] The two systems show significant differences, in particular, with respect to their metal active sites. A large number of studies have been made on the function of the active site of sMMO from various spectroscopic measurements. From quantum chemical calculations, nonradical,[6] radical,[7,8] and nonsynchronous concerted[9] mechanisms have been proposed so far for methane hydroxylation

* To whom correspondence should be addressed. E-mail: kazunari@ms.ifoc.kyushu-u.ac.jp.

(1) Colby, J.; Dalton, H.; Wittenbury, R. *Annu. Rev. Microbiol.* **1979**, *33*, 481.
(2) Anthony, C. *The Biochemistry of Methylotrophs*; Academic Press: London, 1982; pp 296−379.
(3) (a) Feig, A. L.; Lippard, S. J. *Chem. Rev.* **1994**, *94*, 759. (b) Lipscomb, J. D. *Annu. Rev. Microbiol.* **1994**, *48*, 371. (c) Wallar, B. J.; Lipscomb, J. D. *Chem. Rev.* **1996**, *96*, 2625. (d) Que, L., Jr.; Dong, Y. *Acc. Chem. Res.* **1996**, *29*, 190. (e) Merkx, M.; Kopp, D. A.; Sazinsky, M. H.; Blazyk, J. L.; Müller, J.; Lippard, S. J. *Angew. Chem., Int. Ed.* **2001**, *40*, 2782.
(4) Chan, S. I.; Chen, K. H.-C.; Yu, S. S.-F.; Chen, C.-L.; Kuo, S. S.-J. *Biochemistry* **2004**, *43*, 4421.
(5) Lieberman, R. L.; Shrestha, D. B.; Doan, P. E.; Hoffman, B. M.; Stemmler, T. L.; Rosenzeig, A. C. *Proc. Natl. Acad. Sci. U.S.A.* **2003**, *100*, 3820.
(6) (a) Yoshizawa, K.; Yamabe, T.; Hoffmann, R. *New J. Chem.* **1997**, *21*, 151. (b) Yoshizawa, K.; Ohta, T.; Yamabe, T.; Hoffmann, R. *J. Am. Chem. Soc.* **1997**, *119*, 12311. (c) Yoshizawa, K. *J. Biol. Inorg. Chem.* **1998**, *3*, 318. (d) Yoshizawa, K.; Ohta, T.; Yamabe, T. *Bull. Chem. Soc. Jpn.* **1998**, *71*, 1899. (e) Yoshizawa, K.; Suzuki, A.; Shiota, Y.; Yamabe, T. *Bull. Chem. Soc. Jpn.* **2000**, *73*, 815. (f) Yoshizawa, K. *J. Inorg. Biochem.* **2000**, *78*, 23. (g) Yoshizawa, K.; Yumura, T. *Chem.−Eur. J.* **2003**, *9*, 2347. (h) Yoshizawa, K. *Acc. Chem. Res.* **2006**, *39*, 375.
(7) (a) Siegbahn, P. E. M.; Crabtree, R. H. *J. Am. Chem. Soc.* **1997**, *119*, 3103. (b) Siegbahn, P. E. M.; Crabtree, R. H.; Nordlund, P. *J. Biol. Inorg. Chem.* **1998**, *3*, 314. (c) Siegbahn, P. E. M. *Inorg. Chem.* **1999**, *38*, 2880. (d) Siegbahn, P. E. M.; Blomberg, M. R. A. *Chem. Rev.* **2000**, *100*, 421. (e) Siegbahn, P. E. M. *J. Biol. Inorg. Chem.* **2001**, *6*, 27.
(8) (a) Basch, H.; Mogi, K.; Musaev, D. G.; Morokuma, K. *J. Am. Chem. Soc.* **1999**, *121*, 7249. (b) Basch, H.; Musaev, D. G.; Mogi, K.; Morokuma, K. *J. Phys. Chem. A* **2001**, *105*, 3615. (c) Basch, H.; Musaev, D. G.; Morokuma, K. *J. Phys. Chem. B* **2001**, *105*, 8452. (d) Torrent, M.; Musaev, D. G.; Basch, H.; Morokuma, K. *J. Comput. Chem.* **2002**, *23*, 59.
(9) (a) Dunietz, B. D.; Beachy, M. D.; Cao, Y.; Whittington, D. A.; Lippard, S. J.; Friesner, R. A. *J. Am. Chem. Soc.* **2000**, *122*, 2828. (b) Gherman, B. F.; Dunietz, B. D.; Whittington, D. A.; Lippard, S. J.; Friesner, R. A. *J. Am. Chem. Soc.* **2001**, *123*, 3836. (c) Guallar, V.; Gherman, B. F.; Miller, W. H.; Lippard, S. J.; Friesner, R. A. *J. Am. Chem. Soc.* **2002**, *124*, 3377. (d) Baik, M.-H.; Newcomb, M.; Friesner, R. A.; Lippard, S. J. *Chem. Rev.* **2003**, *103*, 2385.

10.1021/ic8003933 CCC: $40.75
Published on Web 12/29/2008

that occurs at the diiron active site. On the other hand, little has been known about the structure of protein and the location of copper active sites of pMMO. Recently, Lieberman and Rosenzweig[10] reported an X-ray crystal structural analysis of pMMO at 2.8 Å resolution. Their excellent work revealed that pMMO consists of three subunits of pmoA, pmoB, and pmoC, which have molecular weights of 24, 47, and 22 kDa, respectively. There are three kinds of metal centers in the crystal structure of pMMO. The pmoB subunit involves a mononuclear copper site and a dinuclear copper site, the distance between the two sites being 21 Å. In the border between pmoA and pmoC, a monozinc site is located 19 Å apart from the dicopper site and 32 Å apart from the monocopper site. Since zinc is contained in the crystallization buffer used and is not detected in X-ray absorption spectroscopy (XAS) measurements,[11] the zinc site is considered to be occupied by a different metal ion such as iron or copper in vivo.

In previous quantum chemical calculations,[6e,12,13] mono-, di-, and tricopper models have been adopted for the active site of pMMO to look at their reactivity to methane. Chan and co-workers[14] proposed an active site that is composed of a trinuclear Cu^{II}Cu^{II}Cu^{II} cluster from X-ray adsorption edge and electron-spin resonance spectroscopic experiments. They suggested that the active site of the X-ray crystal structure should lack the full component of copper ions because it does not display the enzymatic activity. Chen and Chan[13] predicted that a trinuclear Cu^{II}Cu^{II}Cu^{III} complex offers the most facile pathway for methane hydroxylation. Their proposal is of great interest, but the existence of the tricopper site is not established at present from crystal structural analysis. Thus, the question remains to be answered with respect to the real active site for methane hydroxylation by pMMO. In this work, we would like to confine our calculations on the reactivity of the dicopper site to methane.

From density functional theory (DFT) computations, we investigated the reaction pathway and its energetics for the direct methane−methanol conversion by a series of first-row transition-metal oxide species (from Sc to Cu).[15] Late transition-metal oxides, especially FeO^+, NiO^+, and CuO^+, are highly reactive to methane, leading to effective formation of methanol in a nonradical manner. Although CuO^+ can work as a good mediator for the conversion of methane to methanol, the Cu−O bond is so weak that this species has not yet been characterized. On the basis of the X-ray crystal structure (1YEW),[10] we constructed reaction models for the monocopper and dicopper sites using the quantum mechanics/molecular mechanics (QM/MM) technique.[12] The calculations showed that the formation of a dicopper−dioxo species is exothermic, whereas the formation of a monocopper oxo species is endothermic. Thus, the formation of a dicopper active species is favored from an energetic point of view. Although the real active site for methane hydroxylation has not yet been identified from experiments, our previous study suggests that the dicopper species is a likely candidate for the enzymatic function. A number of model complex studies[16−18] based on structural and spectroscopic data also suggest that dicopper species are responsible for the activation of dioxygen and the oxidation of substrate. In the present study, we compare the reactivity of the bis(μ-oxo)Cu^{II}Cu^{III} and bis(μ-oxo)Cu^{III}Cu^{III} species, which can be derived by looking at the surrounding amino acid residues at the dicopper site of pMMO. Although we discuss the reactivity of the dicopper active species to methane in the present work, we cannot rule out the possibility of the tricopper species for methane hydroxylation by pMMO.[14]

Computational Method

Although the B3LYP method[19] has been used in the calculations of various catalytic and enzymatic reactions, this method tends to

(10) (a) Lieberman, R. L.; Rosenzweig, A. C. *Nature* **2005**, *434*, 177. (b) Lieberman, R. L.; Rosenzweig, A. C. *Acc. Chem. Res.* **2007**, *40*, 573.

(11) Lieberman, R. L.; Kondapalli, K. C.; Shrestha, D. B.; Hakemian, A. S.; Smith, S. M.; Telser, J.; Kuzelka, J.; Gupta, R.; Borovik, A. S.; Lippard, S. J.; Hoffman, B. M.; Rosenzweig, A. C.; Stemmler, T. L. *Inorg. Chem.* **2006**, *45*, 8372.

(12) Yoshizawa, K.; Shiota, Y. *J. Am. Chem. Soc.* **2006**, *128*, 9873.

(13) Chen, P. P.-Y.; Chan, S. I. *J. Inorg. Biochem.* **2006**, *100*, 801.

(14) (a) Chen, K. H.-C.; Chen, C.-L.; Tseng, C.-F.; Yu, S. S.-F.; Ke, S. C.; Lee, J.-F.; Nguyen, H.-H. T.; Elliott, S. J.; Alben, J. O.; Chan, S. I. *J. Chin. Chem. Soc.* **2004**, *51*, 1081. (b) Hung, S. C.; Chen, C.-L.; Chen, K. H.-C.; Yu, S. S.-F.; Chan, S. I. *J. Chin. Chem. Soc.* **2004**, *51*, 1229. (c) Chan, S. I.; Wang, V. C.-C.; Lai, J. C.-H.; Yu, S. S.-F.; Chen, P.-Y.; Chen, K. H.-C.; Chen, C.-L.; Chan, M. K. J. *Angew. Chem., Int. Ed.* **2007**, *46*, 1992.

(15) (a) Yoshizawa, K.; Shiota, Y.; Yamabe, T. *Chem.−Eur. J.* **1997**, *3*, 1160. (b) Yoshizawa, K.; Shiota, Y.; Yamabe, T. *J. Am. Chem. Soc.* **1998**, *120*, 564. (c) Shiota, Y.; Yoshizawa, K. *J. Am. Chem. Soc.* **2000**, *122*, 12317.

(16) (a) Pidcock, E.; Obias, H. V.; Zhang, X.; Karlin, K. D.; Solomon, E. I. *J. Am. Chem. Soc.* **1998**, *120*, 7841. (b) Obias, H. V.; Lin, Y.; Murthy, N. N.; Pidcock, E.; Solomon, E. I.; Ralle, M.; Blackburn, N. J.; Neuhold, Y.-M.; Zuberbühler, A. D.; Karlin, K. D. *J. Am. Chem. Soc.* **1998**, *120*, 12960. (c) Kopf, M. A.; Karlin, K. D. Models of Copper Enzymes and Heme-Copper Oxidases. In *Biomimetic Oxidations Catalyzed by Transition Metal Complexes*; Muenier, B., Ed.; Imperial College Press: London, 2000; pp 309−362. (d) Quant Hatcher, L.; Karlin, K. D. *J. Biol. Inorg. Chem.* **2004**, *9*, 669. (e) Lee, Y.; Karlin, K. D. In *Concepts and Models in Bioinorganic Chemistry*; Metzler-Nolte, N., Kraatz, H.-B., Eds.; Wiley-VCH: Weinheim, Germany, 2006; pp 363−395. (f) Hatcher, L. Q.; Karlin, K. D. *Adv. Inorg. Chem.* **2006**, *58*, 131.

(17) (a) Halfen, J. A.; Mahapatra, S.; Wilkinson, E. C.; Kaderli, S.; Young, V. G., Jr.; Que, L., Jr.; Zuberbüler, A. D.; Tolman, W. B. *Science* **1996**, *271*, 1397. (b) Mahapatra, S.; Halfen, J. A.; Wilkinson, E. C.; Pan, G.; Wang, X.; Young, V. G., Jr.; Cramer, C. J.; Que, L., Jr.; Tolman, W. B. *J. Am. Chem. Soc.* **1996**, *118*, 11555. (c) Mahapatra, S.; Young, V. G., Jr.; Kaderli, S.; Zuberbüler, A. D.; Tolman, W. B. *Angew. Chem., Int. Ed. Engl.* **1997**, *36*, 130. (d) Que, L., Jr.; Tolman, W. B. *Angew. Chem., Int. Ed.* **2002**, *41*, 1114. (e) Aboelella, N. W.; Lewis, E. A.; Reynolds, A. M.; Brennessel, W. W.; Cramer, C. J.; Tolman, W. B. *J. Am. Chem. Soc.* **2002**, *124*, 10660. (f) Aboelella, N. W.; Kryatov, S. V.; Gherman, B. F.; Brennessel, W. W.; Young, V. G.; Sarangi, R.; Rybak-Akimova, E. V.; Hodgson, K. O.; Hedman, B.; Solomon, E. I.; Cramer, C. J.; Tolman, W. B. *J. Am. Chem. Soc.* **2004**, *126*, 16896. (g) Sarangi, R.; Aboelella, N.; Fujisawa, K.; Tolman, W. B.; Hedman, B.; Hodgson, K. O.; Solomon, E. *J. Am. Chem. Soc.* **2006**, *128*, 8286. (h) Brown, E. C.; Bar-Nahum, I.; York, J. T.; Aboelella, N. W.; Tolman, W. B. *Inorg. Chem.* **2007**, *46*, 486. (i) Hong, S.; Huber, S. M.; Gagliardi, L.; Cramer, C. C.; Tolman, W. B. *J. Am. Chem. Soc.* **2007**, *129*, 14190.

(18) (a) Itoh, S.; Nakao, H.; Berreau, L. M.; Kondo, T.; Komatsu, M.; Fukuzumi, S. *J. Am. Chem. Soc.* **1998**, *120*, 2890. (b) Taki, M.; Itoh, S.; Fukuzumi, S. *J. Am. Chem. Soc.* **2001**, *123*, 6203. (c) Itoh, S.; Kumei, H.; Taki, M.; Nagatomo, S.; Kitagawa, T.; Fukuzumi, S. *J. Am. Chem. Soc.* **2001**, *123*, 6708. (d) Itoh, S.; Fukuzumi, S. *Bull. Chem. Soc. Jpn.* **2002**, *75*, 2081. (e) Osako, T.; Ohkubo, K.; Taki, M.; Tachi, Y.; Fukuzumi, S.; Itoh, S. *J. Am. Chem. Soc.* **2003**, *125*, 11027. (f) Itoh, S. Dicopper Enzymes. In *Comprehensive Coordination Chemistry II*; Que, L., Jr., Tolman, W. B., Eds.; Elsevier: Amsterdam, 2004; Vol. *8*, pp 369−393. (g) Itoh, S.; Tachi, Y. *Dalton Trans.* **2006**, 4531.

(19) Becke, A. D. *J. Chem. Phys.* **1993**, *98*, 5648.

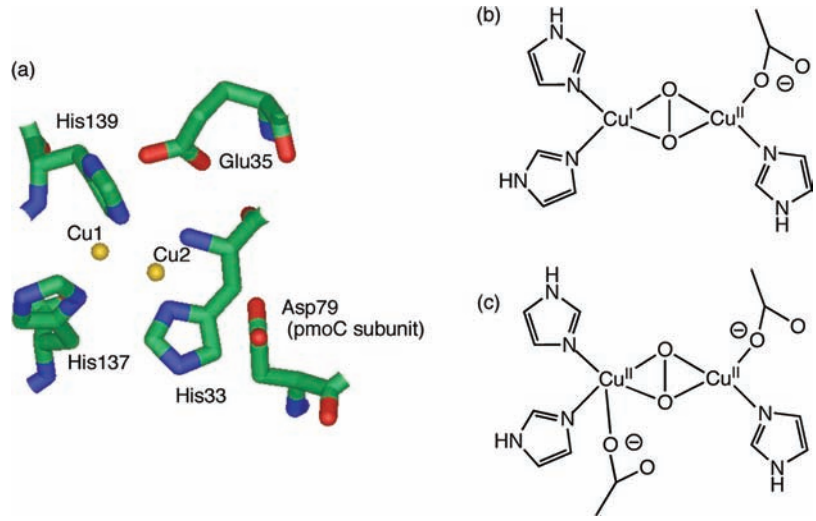

Figure 1. (a) X-ray structure of the dicopper site in the pmoB subunit and charge-neutral models of (b) $Cu^{I}Cu^{II}$ and (c) $Cu^{II}Cu^{II}$ peroxo species.

overestimate the spin-state splitting.[20] Thus, it is difficult to estimate the accurate energy difference between high-spin and low-spin states in computations at the B3LYP level of theory. The B3LYP energy expression is in the form of eq 1:

$$E_{XC}^{\mathrm{B3LYP}} = (1 - a_0)E_X^{\mathrm{LSDA}} + a_0 E_X^{\mathrm{HF}} + a_x E_X^{\mathrm{B88}} + a_c E_C^{\mathrm{LYP}} + (1 - a_c)E_C^{\mathrm{VWN}} \quad (1)$$

$$a_0 = 0.20, \quad a_x = 0.72, \quad a_c = 0.81$$

E_X^{HF} is the Hartree−Fock exchange energy; E_X^{LSDA} is the local exchange energy from the local spin density approximation (LSDA); E_X^{B88} is Becke's gradient correction[21] to the exchange functional; E_C^{B3LYP} is the correlation functional developed by Lee, Yang, and Parr;[22] and E_C^{VWN} is the correlation energy calculated using the local correlation functional of Vosko, Wilk, and Nusair (VWN).[23] Reiher and co-workers[20] reported that the B3LYP hybrid functional using a parameter a_0 of 0.15 can improve the energy difference between different spin states. Thus, we used the reparametrized B3LYP method, denoted as B3LYP*, to optimize local minima and saddle points on the potential energy surfaces. Even in spin singlet-state calculations, we used the spin-unrestricted method that can allow breaking the symmetry of the wave functions for α and β spin. It is a reasonable choice for describing the antiferromagnetic state for the dicopper species. All singlet energies from the unrestricted calculations were computed using the raw broken-symmetry SCF energy without modification. We used the (16s10p6d) primitive set of Wachters−Hay[24,25] supplemented with one polarization f function (α = 1.44 for Cu)[26] for the Cu atoms and the D95** basis set[27] for the H, C, and O atoms. The program we used is Gaussian 03.[28] After geometry optimizations, we performed vibrational analyses to confirm that an optimized geometry corresponds to a local minimum that has no imaginary frequency or a transition state that has only one imaginary frequency. The zero-point vibrational energies were calculated using the harmonic approximation. The Gibbs free energies were obtained at 298.15 K.

Results and Discussion

Dicopper Complexes. We considered two kinds of initial peroxo species for methane hydroxylation at the dicopper active site of pMMO, as shown in Figure 1. The two initial peroxo species are the mixed-valent $Cu^{I}Cu^{II}$ state in the doublet state and the $Cu^{II}Cu^{II}$ state in the singlet state. Charge neutrality imposed is important in correctly considering the reactivity because, in our experience, the reaction of methane with metal−oxo species is significantly affected by the total charge of system.[29] For example, the cationic complexes of FeO^{+} and FeO^{2+} can effectively activate methane, whereas the neutral complex of FeO hardly reacts with methane. Moreover, the binding energies between FeO^{n+} (n = 0, 1, and 2) and methane strongly depend on the total charges of the systems; in fact, the binding energies are 5.7 (n = 0), 22.8 (n = 1), and 70.3 kcal/mol (n = 2) at the B3LYP/6-311G** level. To avoid such important charge effects, we assumed one and two of Glu35 and Asp79 to coordinate to the $Cu^{I}Cu^{II}$ and $Cu^{II}Cu^{II}$ species, respectively, at the dicopper site of pMMO, as shown in Figure 1. We used acetate as a model of the Glu35 and Asp79 residues and imidazole as a model of the three histidine residues.

It is difficult to describe the singlet potential energy surface within the framework of the spin-restricted method because the peroxo $Cu^{II}Cu^{II}$ species should have antiferromagnetic coupling of the d^9 electronic configuration. Therefore, we cannot reasonably impose a closed-shell electronic configuration to such an open-shell system. For open-shell singlet energies, we used the raw broken-symmetry SCF energy, in which the triplet component is not projected out. The energy

(20) (a) Reiher, M.; Salomon, O.; Hess, B. A. *Theor. Chem. Acc.* **2001**, *107*, 48. (b) Salomon, O.; Reiher, M.; Hess, B. A. *J. Chem. Phys.* **2002**, *117*, 4729.
(21) Becke, A. D. *Phys. Rev. A* **1988**, *38*, 3098.
(22) Lee, C.; Yang, W.; Parr, R. G. *Phys. Rev. B* **1988**, *37*, 785.
(23) Vosko, S. H.; Wilk, L.; Nusair, M. J. *Can. J. Phys.* **1980**, *58*, 1200.
(24) Wachters, A. J. H. *J. Chem. Phys.* **1970**, *52*, 1033.
(25) Hay, P. J. *J. Chem. Phys.* **1977**, *66*, 4377.
(26) Raghavachari, K.; Trucks, G. W. *J. Chem. Phys.* **1989**, *91*, 1062.
(27) Dunning, T. H.; Hay, P. J. In *Modern Theoretical Chemistry*; Schaefer, H. F., III, Ed.; Plenum: New York, 1976; Vol. *3*, pp 1−27.
(28) Frisch, M. J. et al. *Gaussian 03*, revision E.01; Gaussian, Inc.: Wallingford, CT, 2004.
(29) Yoshizawa, K.; Shiota, Y.; Yamabe, T. *Organometallics* **1998**, *17*, 2825.

Table 1. Calculated Mulliken Spin Densities (Atomic Charges) in the Cu_2O_2 Core

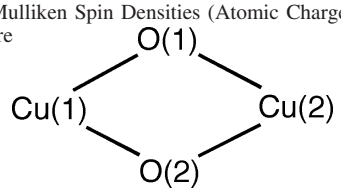

	spin state	$<S^2>^c$	Cu(1)	Cu(2)	O(1)	O(2)
1	doublet	0.750	0.02 (0.06)	0.37 (0.37)	0.24 (−0.38)	0.29 (−0.39)
2	doublet	0.750	0.48 (0.34)	−0.08 (0.38)	0.30 (−0.50)	0.25 (−0.63)
3	singlet[a]	0.038	0.52 (0.35)	−0.44 (0.42)	0.00 (−0.28)	0.00 (−0.27)
4	singlet[b]	0.000	0.00 (0.38)	0.00 (0.38)	0.00 (−0.45)	0.00 (−0.44)
5	singlet[a]	0.172	0.59 (0.34)	0.04 (0.34)	−0.81 (−0.35)	−0.04 (−0.46)

[a] Open-shell singlet. [b] Closed-shell singlet. [c] $<S^2>$ after annihilation.

difference between the spin-restricted method and the spin-unrestricted method was calculated to be 3.7 kcal/mol at the BLYP level and 14.7 kcal/mol at the B3LYP* level. Although the energy difference is small at the BLYP level,[30] the closed-shell singlet is clearly inappropriate for the peroxo complex at the B3LYP* level. To ensure that the broken-symmetry calculations were carried out correctly, we traced calculated spin densities for the following dicopper−dioxygen species of μ-η^1:η^2-peroxoCu^ICu^{II} (**1**), bis(μ-oxo)$Cu^{II}Cu^{III}$ (**2**), μ-η^2:η^2-peroxo$Cu^{II}Cu^{II}$ (**3**), and μ-oxo$Cu^{III}Cu^{III}$ (**5**), as listed in Table 1. On the other hand, the bis(μ-oxo)$Cu^{III}Cu^{III}$ species (**4**) is a couple of the d^8 electronic configuration, and, therefore, it is a diamagnetic closed-shell species, which is reasonably treated within the framework of the spin-restricted methodology. We also calculated **3** and **5** in the triplet state.

Figure 2 shows optimized structures of **1** and **2** in the doublet state and **3**, **4**, and **5** in the singlet state. Although we expected the μ-η^2:η^2-peroxo form to be obtained for the peroxo Cu^ICu^{II} species (**1**), what we obtained from B3LYP* calculations is the μ-η^1:η^2-peroxo form. The O(1)−O(2) bond distance of 1.456 Å is reasonable for a peroxo species, whereas the O−O double bond distance is 1.207 Å in the dioxygen molecule. The Cu(1)−O(1) bond distance of 2.252 Å is slightly longer than those of Cu(2)−O(1) and Cu(2)−O(2) bonds, which are 1.961 and 1.923 Å, respectively. The dioxygen moiety of **1** is tightly bound to the Cu(2) atom, in comparison with the Cu(1) atom. In contrast to the Cu−O bonds, the two Cu(1)−N bonds are shorter than the Cu(2)−N bond. The O−O bond cleavage occurs in **1** concomitant with the formation of the Cu(1)−O(2) bond, resulting in the formation of a bis(μ-oxo) form. The Cu(1)−O(2) distance is remarkably decreased to 1.931 Å, and the O(1)−O(2) and the Cu(1)−Cu(2) bond distances are 2.409 and 2.742 Å, respectively, in **2**.

We next consider the peroxo $Cu^{II}Cu^{II}$ complex that has a μ-η^2:η^2-peroxo form. The O−O distance of 1.448 Å is quite similar to that of **1**, whereas the Cu(1)−Cu(2) distance of 3.261 Å in **3** is much shorter than the Cu(1)−Cu(2) distance of 4.157 Å in **1**. The four Cu−O bond distances range from 1.9 to 2.1 Å in the Cu_2O_2 core. The cleavage of the O(1)−O(2) bond in **3** is responsible for the formation of the bis(μ-oxo)$Cu^{III}Cu^{III}$ species **4**. As a result, the O(1)−O(2) distance increases from 1.448 Å in **3** to 2.302 Å in **4**. The Cu(1)−Cu(2) distance decreases to 2.663 Å in **4**. In addition to the O(1)−O(2) bond dissociation, the Cu(1)−O(1) bond dissociation occurs in **4**, resulting in the formation of a μ-oxo$Cu^{III}Cu^{III}$ isomer, **5**. The Cu_2O_2 core involves a bridged oxo ligand and a nonbridged oxo ligand. The nonbridged oxygen forms a Cu−O bond of 1.772 Å, whereas the bridged oxygen retains two Cu−O bonds of 1.895 and 1.795 Å.

Since the energy difference between **1** and **2** is only 2.5 kcal/mol, the interconversion between the μ-η^1:η^2-peroxo-Cu^ICu^{II} species and the bis(μ-oxo)$Cu^{II}Cu^{III}$ species is likely to occur under ambient conditions. In contrast, a calculated energy of **4** is 14.1 kcal/mol and that of **5** is 21.0 kcal/mol, relative to **3** in the singlet state. Thus, the formation of the bis(μ-oxo)$Cu^{III}Cu^{III}$ and μ-oxo$Cu^{III}Cu^{III}$ species is unlikely to occur, compared to the formation of the bis(μ-oxo)$Cu^{II}Cu^{III}$ species, from a viewpoint of energy. The triplet-state energies of **3** and **5**, relative to the singlet state of **3**, are −0.39 and 20.1 kcal/mol, respectively. Since these values are in line with those of the relevant open-shell singlet states, the result remains unchanged in the triplet state. Cramer et al.[30] reported the bis(μ-oxo)$Cu^{III}Cu^{III}$ species to be 8.3 kcal/mol at the BLYP/TZP level and 27.3 kcal/mol at the B3LYP/TZP level above the peroxo$Cu^{II}Cu^{II}$ species using a small model of $(Cu_2O_2)(imid)_6$ in the singlet state. The corresponding energy difference of 14.1 kcal/mol in our calculations at the B3LYP* level lies between 8.3 kcal at the BLYP level and 27.3 kcal/mol at the B3LYP level. The B3LYP* (a_0 = 0.15) result reasonably lies between the pure BLYP (a_0 = 0) result and the hybrid B3LYP (a_0 = 0.20) result. Note that the increase of the HF exchange in the functional of eq 1 tends to overestimate the spin-state splitting of the bis(μ-oxo)$Cu^{III}Cu^{III}$ species. In any case, the bis(μ-oxo)$Cu^{III}Cu^{III}$ species is calculated to lie above the corresponding μ-η^2:η^2-peroxo$Cu^{II}Cu^{II}$ species at these DFT levels of theory. In contrast to these results, Flock and Pierloot[31] reported the bis(μ-oxo)$Cu^{III}Cu^{III}$ species to be 12.7 kcal/mol below the μ-η^2:η^2-peroxo$Cu^{II}Cu^{II}$ species at the CASPT2 level of theory using a simple model of $(Cu_2O_2)(NH_3)_6$. Recently, Gherman and Cramer[32] pointed out that this prediction at the CASPT2 level is not fully correct because of error in the second-order perturbation (PT2) correction.

To gain a better understanding of the electronic structures of these dicopper−dioxygen species, let us look at useful information from the Mulliken population analysis listed in Table 1. The spin density distribution directly reflects the electronic features along the reaction pathway from the peroxo species to the dioxo species. The spin densities at the Cu(1) and Cu(2) atoms are computed to be 0.02 and 0.37 in **1**, respectively, while those at the Cu(1) and Cu(2) atoms are 0.48 and −0.08 in **2**, respectively. The remaining spin densities in both species are distributed on the two oxygen atoms of the Cu_2O_2 core. The present Mulliken population analysis reasonably indicates that the formal charges of the Cu(1) and Cu(2) atoms should be viewed as +1 and +2 in

(30) (a) Cramer, C. J.; Woloch, M.; Piecuch, P.; Puzzarini, C.; Gagliardi, L. *J. Phys. Chem. A* **2006**, *110*, 1991. (b) Cramer, C. J.; Kinal, A.; Woloch, M.; Piecuch, P.; Gagliardi, L. *J. Phys. Chem. A* **2006**, *110*, 11557. (c) Lewin, J. L.; Heppner, D. E.; Cramer, C. J. *J. Biol. Inorg. Chem.* **2007**, *12*, 1221.

(31) Flock, M.; Pierloot, K. *J. Phys. Chem. A* **1999**, *103*, 95.

(32) Gherman, B. F.; Cramer, C. J. *Coord. Chem. Rev.* **2008**, in press.

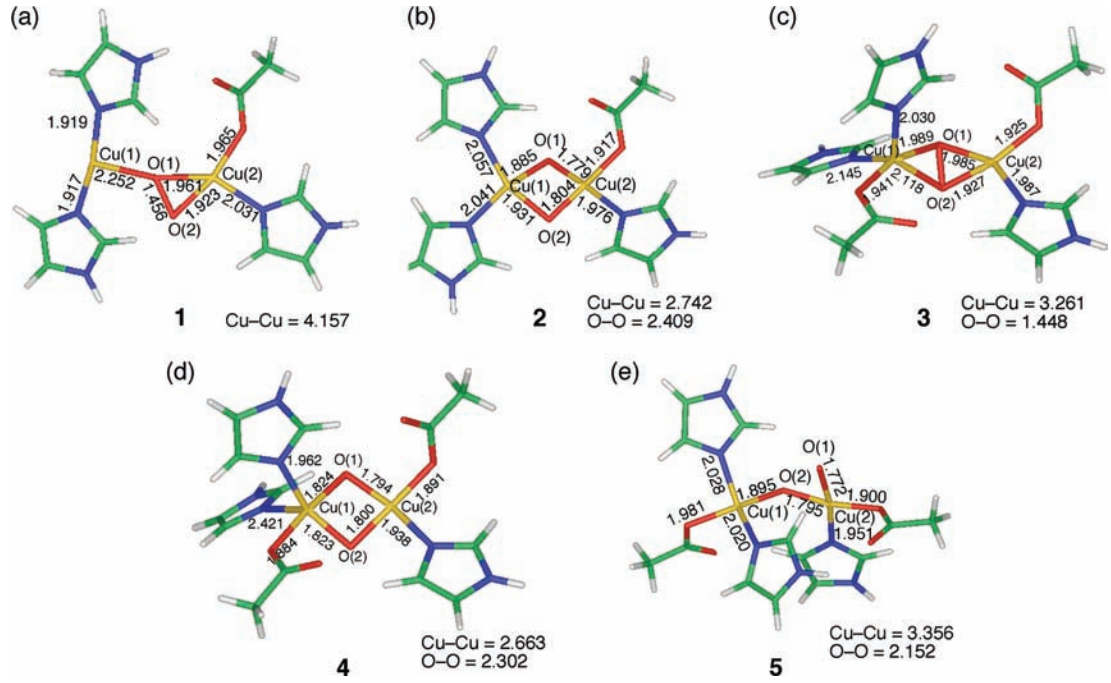

Figure 2. Optimized structures of (a) μ-η^1:η^2-peroxoCu^{I}Cu^{II} **1**, (b) bis(μ-oxo)Cu^{II}Cu^{III} **2**, (c) μ-η^2:η^2-peroxoCu^{II}Cu^{II} **3**, (d) bis(μ-oxo)Cu^{III}Cu^{III} **4**, and (e) μ-oxoCu^{III}Cu^{III} **5**.

1 and +2 and +3 in **2**, respectively. This result is reasonable because the Cu(2) atom is coordinated by a negatively charged ligand. Complex **3** takes an open-shell singlet state because the two copper atoms are of d^9 configuration, the two being antiferromagnetically coupled. The spin densities of the Cu(1) and Cu(2) atoms in **3** are computed to be 0.52 and −0.44 in the open-shell singlet. Since the closed-shell singlet state lies well below the triplet state in **4**, there is no spin density in the Cu_2O_2 core. When one of the Cu−O bonds is broken, large spin densities are induced in the Cu_2O_2 core. In the open-shell singlet state of **5**, the nonbridged oxygen atom carries a large spin density of −0.81, whereas the bridged oxygen atom has almost no spin density. The nonbridged Cu(2)O(1) moiety is similar to the bare CuO^+ complex, which is a highly reactive species and a good oxygen donor because of the small bond dissociation energy of about 30 kcal/mol.[14c,33] The CuO^+ species can be viewed as a Cu^{II} oxyl species because of the large spin density of Cu(2). These results are fully consistent with recent DFT calculations.[17i,34−36] Thus, complex **5** might be viewed as a reactive species of pMMO.

C−H Bond Activation of Methane by the Dicopper Complexes. Let us next look at the reactivity of the dicopper−dioxygen species with respect to the hydroxylation of methane. First of all, we should mention from DFT calculations that the peroxo species of **1** and **3** have no direct ability to activate methane. We think that the peroxo species should be viewed as a precursor of real active species. Figure 3 shows energy diagrams along the reaction pathway starting from **1**, relative to the dissociation limit (**1** and methane) in the doublet state. The reaction of **2** with methane is discussed in detail in a previous paper.[12] The hydroxylation of methane by **2** starts with the formation of a methane complex, in which methane is weakly bound to the copper complex with a binding energy of 0.6 kcal/mol at the B3LYP* level of theory. The small binding energy is reasonable for the interaction between alkane and charge-neutral, metal−oxo species: 5.7 kcal/mol (FeO ($^6\Sigma^+$) and methane)[29] and 3.4 kcal/mol (the so-called α-oxygen species of Fe-ZSM-5 zeolite and methane).[37] The weak interaction between these metal−oxo species and methane is attributed to the low acidity and basicity of methane and the lack of dipole moment.

The first transition state (**TS1**) is related to the important electronic process that leads to the C−H bond dissociation of methane. A calculated relative energy of **TS1** is 16.1 kcal/mol, compared with the dissociation limit. This H-atom abstraction results in the formation of the methyl intermediate; no radical species is formed in this mechanism. This mechanical proposal is consistent with the experimental observation[38] that chiral ethane hydroxylation by pMMO from *Methylococcus capsulatus* (Bath) exhibits negligible racemization. The energy diagram connects the methyl intermediate and the methanol complex via the second transition state (**TS2**) that leads to the formation of the C−O bond of methanol. **TS2** lies 24.3 kcal/mol above the dissociation limit of **1** and methane. Considering the computational result that **TS2** lies 8.2 kcal/mol above **TS1**, the

(33) Yoshizawa, K.; Kihara, N.; Kamachi, T.; Shiota, Y. *Inorg. Chem.* **2006**, *45*, 3034.
(34) Schröder, D.; Holthausen, M. C.; Schwarz, H. *J. Phys. Chem. B* **2004**, *108*, 14407.
(35) Solomon, E. I.; Decker, A. *Curr. Opin. Chem. Biol.* **2005**, *9*, 152.
(36) Comba, P.; Knoppe, S.; Martin, B.; Rajaraman, G.; Rolli, C.; Shapiro, B.; Stork, T. *Chem.—Eur. J.* **2008**, *14*, 344.
(37) Yoshizawa, K.; Shiota, Y.; Yumura, T.; Yamabe, T. *J. Phys. Chem. B* **2000**, *104*, 734.
(38) Wilkinson, B.; Zhu, M.; Priestley, N. D.; Nguyen, H.-H. T.; Morimoto, H.; Williams, P. G.; Chan, S. I.; Floss, H. G. *J. Am. Chem. Soc.* **1996**, *118*, 921.

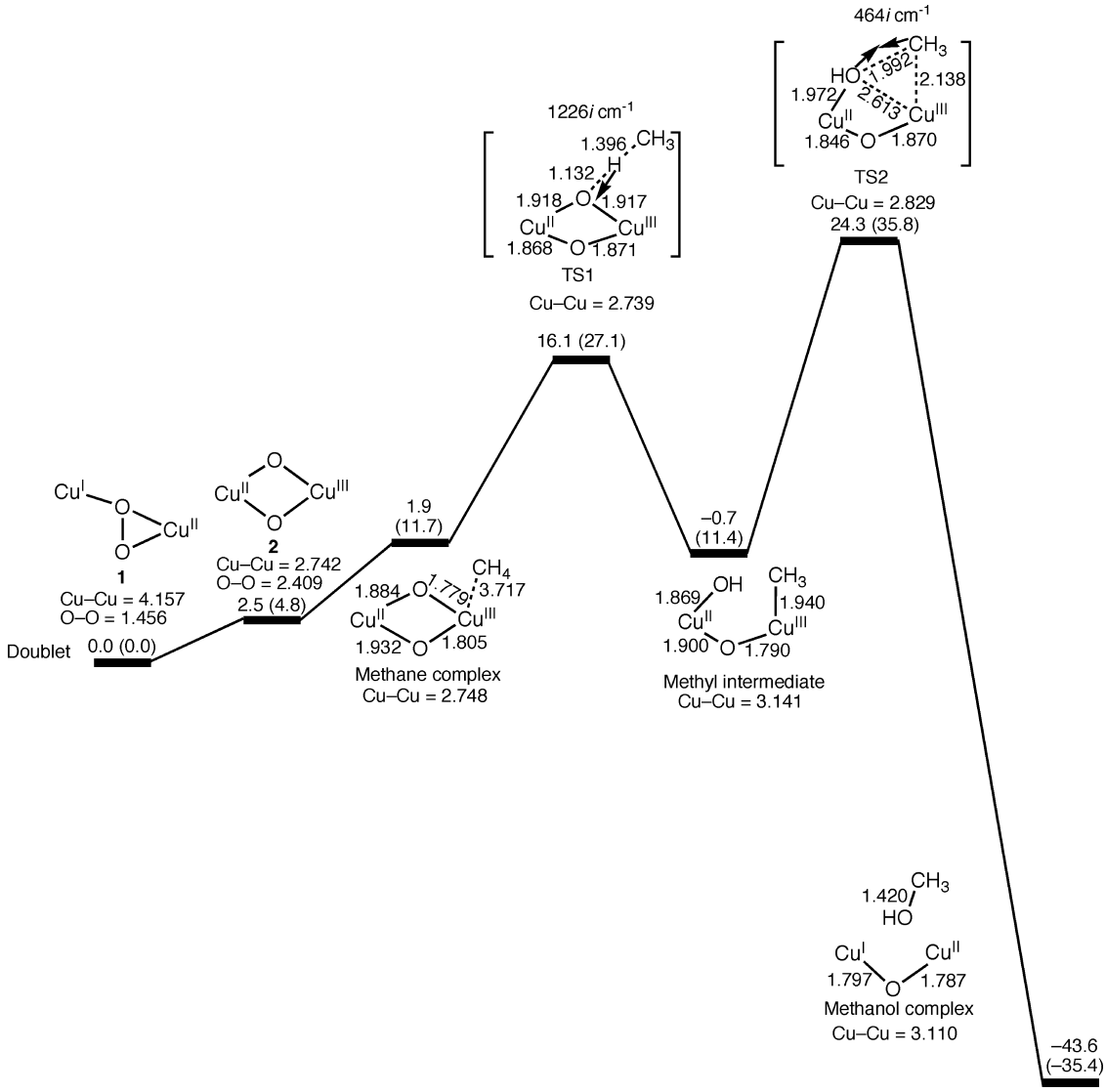

Figure 3. Energy diagram (electronic) for methane hydroxylation starting from **1**. The energies are corrected by zero-point vibrational energies and Gibbs free energies. Values in parentheses are Gibbs free energies. Units are in kcal/mol and Å.

rate-determining step is not the C−H bond dissociation step in the methane hydroxylation catalyzed by the bis(μ-oxo)Cu^{II}Cu^{III} species. These calculated activation barriers are not consistent with experimental observation of KIE (k_H/k_D) values of 5.2−5.5 at 30 °C in ethane hydroxylation by pMMO, which shows that the rate-determining step is clearly the C−H bond-activation step.[38] The protein environment is expected to play an important role in the C−O bond formation by decreasing the activation barrier of **TS2**. In fact, the OH migration in the catalysis of B_{12}-dependent diol dehydratase is significantly affected by surrounding amino acid residues at the active site.[39] The transition state for the OH migration is significantly decreased in energy when the protein environment is taken into account, whereas it is higher than the transition state for the H-atom abstraction of the first step when the protein environment is not considered. For a better understanding of the structure−reactivity correlation of pMMO, we need to fully consider the protein environment at the dicopper site of pMMO in future work.

Let us next look at the methane-to-methanol conversion that starts from **3**. Figure 4 shows calculated relative energies of **3**, **4**, and **5** and the reaction species along the reaction pathway in the singlet state. We partly adopted the spin-unrestricted methodology for the open-shell singlet systems, in which the two copper ions are antiferromagnetically coupled. To check the validity of the open-shell singlet calculations, we looked at calculated spin densities of the singlet state in detail. The dissociation of the O−O bond of **3** leads to the formation of **4**, for which the closed-shell singlet state becomes the ground state. The cleavage of a Cu−O bond in the Cu_2O_2 core results in the formation of **5**, where spin density is localized at the nonbridged oxygen atom, as mentioned earlier. The nonbridged oxygen atom in **5** can abstract a H atom of methane after the formation of methane complex **2**, which has a binding energy of 0.6 kcal/mol at the B3LYP* level. The activation energy for **TS3** is calculated to be 9.5 kcal/mol, relative to this methane

(39) (a) Kamachi, T.; Toraya, T.; Yoshizawa, K. *J. Am. Chem. Soc.* **2004**, *126*, 16207. (b) Kamachi, T.; Toraya, T.; Yoshizawa, K. *Chem.—Eur. J.* **2007**, *13*, 7864.

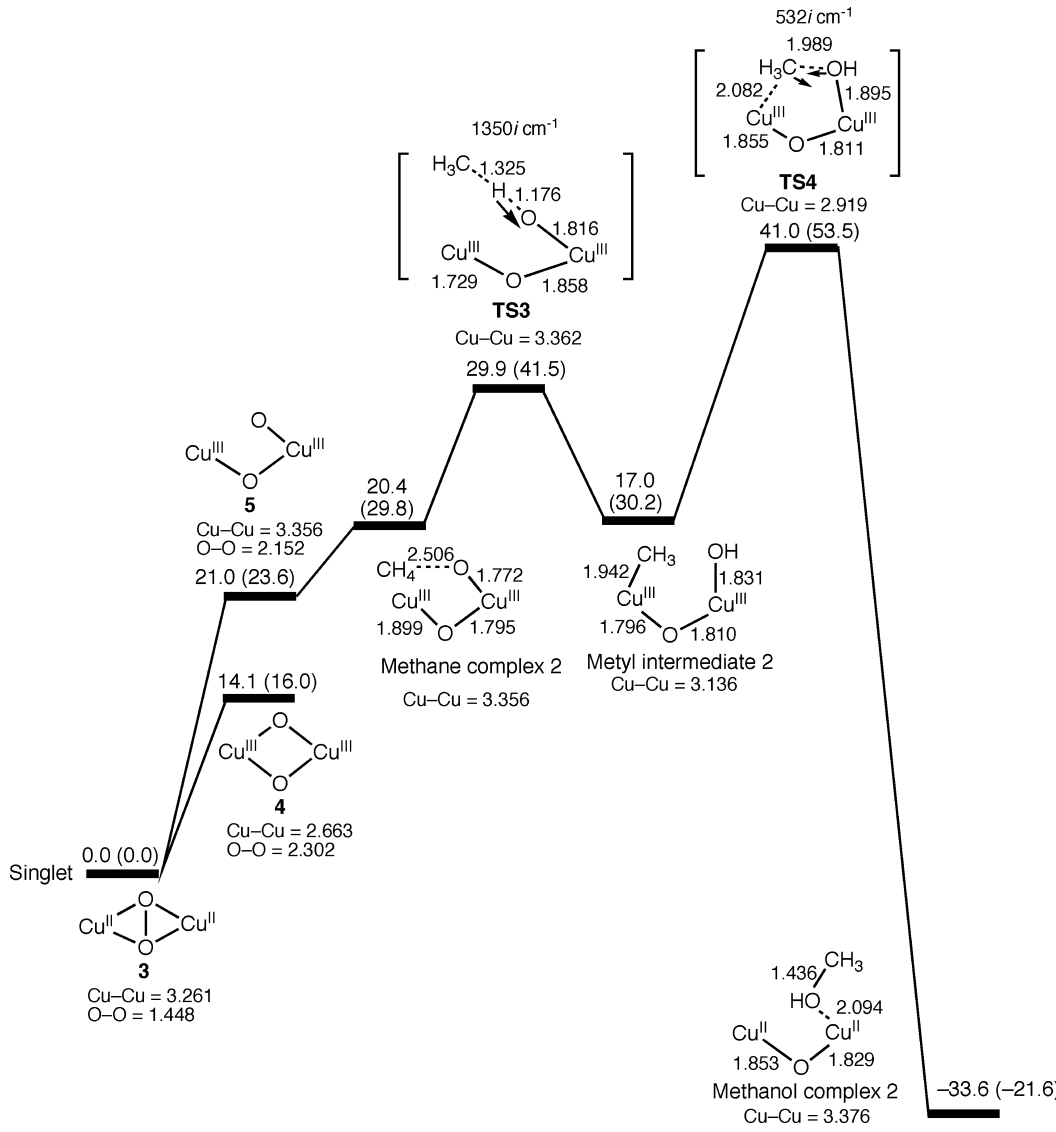

Figure 4. Energy diagram for methane hydroxylation starting from **3**. The energies are corrected by zero-point vibrational energies and Gibbs free energies. Values in parentheses are Gibbs free energies. Units are in kcal/mol and Å.

complex. After this transition state, methyl intermediate **2** is formed. The energy diagram connects methyl intermediate **2** and methanol complex **2** via **TS4**. The two energy diagrams shown in Figures 3 and 4 have similar profiles in that the second transition state lies in energy above the first transition state; the second steps are a highly downhill process with an exothermal energy of about 50 kcal/mol. This thermal energy derives from the formation of a C−O bond and can promote the release of methanol from the methanol complexes.

Considering the C−H bond dissociation energy of 104 kcal/mol for methane in the gas phase, the calculated results tell us that methane is highly activated by these copper oxo complexes (**2** and **5**), leading to a decrease in activation barrier for the C−H bond dissociation. However, there is a significant difference in the relative energies of **2** and **5**, measured from the relevant peroxo complexes. The formation of **2** and **5** are calculated to be 2.5 and 21.0 kcal/mol, relative to the corresponding peroxo species, respectively. The formation of **2** is energetically favored, due to the easier cleavage of the O−O bond in **1**. Therefore, **2** plays an important role in the C−H bond activation for the conversion of methane to methanol by the dicopper site of pMMO. Recently, York et al. reported that replacement of a Cu^{III} ion in the $[Cu_2(\mu\text{-}O)_2]$ core with a different metal ion has important electronic, structural, and reactivity consequences in experiments and theoretical calculations.[40] Their work suggests that the reactivity of the bis(μ-oxo) dicopper complexes strongly depends on the oxidation state of Cu ion in the $[Cu_2(\mu\text{-}O)_2]$ core. The reactive bis(μ-oxo)$Cu^{II}Cu^{III}$ species can be created either from the electron injection to the bis(μ-oxo)$Cu^{III}Cu^{III}$ species or from the O−O bond cleavage in the μ-η^1:η^2-peroxo$Cu^{I}Cu^{II}$ species. Although the role of the other metal sites remains unknown, these may play a role in the electron transfer. At present, however, we confined the discussion about the dinuclear Cu site to after the formation of **1** or **3**. This treatment is sufficient for a better understanding of the C−H activation of methane by pMMO.

Finally, we would like to comment on the concerted reaction pathway for methane hydroxylation by the bis(μ-

(40) York, J. T.; Llobet, A.; Cramer, C. J.; Tolman, W. B. *J. Am. Chem. Soc.* **2007**, *129*, 7990.

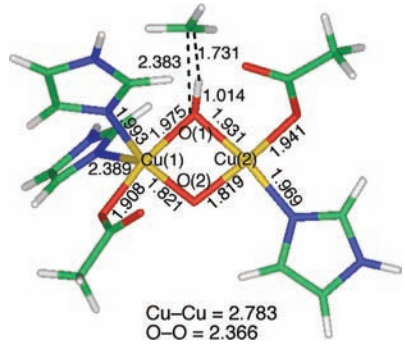

Figure 5. Optimized geometry for the transition state for direct oxygen insertion in the singlet state. Units are in Å.

oxo)Cu^{III}Cu^{III} species. We found a transition state for the direct oxygen insertion into a C−H bond of methane, as shown in Figure 5. Although the imaginary frequency of 703*i* cm^{-1} in the transition state can be viewed as a C−H stretching mode, the obtained C−H distance of 1.731 Å and O−H distance of 1.014 Å indicate that this transition state is very late. This means that the C−H bond is almost cleaved and the O−H bond is already formed in this transition state. The C−O bond distance is calculated to be 2.383 Å. These geometrical features suggest that this transition state can be separated into a methyl radical and a $Cu_2O(OH)$ species. The electronic structure of this transition state possesses internal instability with regard to the spin-restricted solution for the Kohn−Sham equation. We confirmed that the concerted transition state transforms into **5** in the open-shell singlet state. In fact, since the activation energy ($\Delta E^{\ddagger}$) and the activation free energy ($\Delta G^{\ddagger}$) of this reaction are computed to be 44.0 and 54.8 kcal/mol, respectively, we can reasonably rule out this concerted reaction pathway for direct oxygen insertion.

Conclusions

We have considered the reaction mechanism of methane hydroxylation by two kinds of dicopper−dioxygen species that can be viewed as possible active species of pMMO using the B3LYP* method. The peroxo species of Cu^{I}Cu^{II} and Cu^{II}Cu^{II} are transformed into the bis(μ-oxo) species of Cu^{II}Cu^{III} and Cu^{III}Cu^{III}, respectively. The mixed-valent peroxo Cu^{I}Cu^{II} species and the corresponding bis(μ-oxo)Cu^{II}Cu^{III} species are close in energy; thus, the interconversion between the two species easily occurs in the mixed-valent dicopper species. In contrast, the peroxo Cu^{II}Cu^{II} species lies well below the corresponding bis(μ-oxo)Cu^{III}Cu^{III} species. Since the peroxo Cu^{II}Cu^{II} species is energetically preferred, the O−O bond dissociation is unlikely to occur, in comparison with the mixed-valent peroxo Cu^{I}Cu^{II} species. We calculated the energy profile for the conversion of methane to methanol by these Cu_2O_2 species. The activation barrier for the C−H bond dissociation is 16.1 kcal/mol in the bis(μ-oxo)Cu^{II}Cu^{III} species, whereas neither the bis(μ-oxo)Cu^{III}Cu^{III} species nor the μ-oxoCu^{III}Cu^{III} species is likely to mediate the C−H bond activation of methane. We considered another pathway for the concerted oxygen insertion in the bis(μ-oxo)Cu^{III}Cu^{III} species. Since the activation barrier for the concerted pathway is computed to be 44.0 kcal/mol, we reasonably ruled out this pathway. Finally, we predict that the reactivity to methane is increased by the bis(μ-oxo)Cu^{III}Cu^{III}, μ-oxoCu^{III}Cu^{III}, and bis(μ-oxo)Cu^{II}Cu^{III} species in this order; as a result, we think that the bis(μ-oxo)Cu^{II}Cu^{III} species should play an important role in methane activation by pMMO.

Acknowledgment. This work was supported by Grants-in-Aid for Scientific Research (Grant Nos. 18350088, 18066013, and 18GS0207) from the Japan Society for the Promotion of Science; the Global COE Project; the Nanotechnology Support Project; the Joint Project of Chemical Synthesis Core Research Institutions from the Ministry of Culture, Sports, Science, and Technology of Japan (MEXT); and CREST of the Japan Science and Technology Cooperation.

Supporting Information Available: Complete ref 28 and atomic Cartesian coordinates for all the structures optimized in the present study. This material is available free of charge via the Internet at http://pubs.acs.org.

IC8003933